Two-dimensional localization in GeSn

OPEN ACCESS
IOP Publishing
Journal of Physics: Condensed Matter
J. Phys.: Condens. Matter **34** (2022) 485301 (8pp)
https://doi.org/10.1088/1361-648X/ac9814

Two-dimensional localization in GeSn

Y Gul[1], S N Holmes[2,*], Chang-Woo Cho[3], B Piot[3], M Myronov[4,*] and M Pepper[1,2]

[1] London Centre for Nanotechnology, University College London, 17-19 Gordon Street, London WC1H 0AH, United Kingdom
[2] Department of Electronic and Electrical Engineering, University College London, Torrington Place, London WC1E 7JE, United Kingdom
[3] LNCMI-CNRS, Grenoble 38042, France
[4] Department of Physics, University of Warwick, Coventry CV4 7AL, United Kingdom

E-mail: stuart.holmes@ucl.ac.uk and m.myronov@warwick.ac.uk

Received 25 July 2022, revised 16 September 2022
Accepted for publication 6 October 2022
Published 13 October 2022

Abstract

Localization behaviour is a characteristic feature of the *p*-type GeSn quantum well (QW) system in a metal–insulator–semiconductor device. The transition to strongly localized behaviour is abrupt with thermally activated conductivity and a high temperature intercept of $0.12 \times e^2\,\hbar^{-1}$ at a hole carrier density 1.55×10^{11} cm^{-2}. The activation energy for the conductivity in the localized state is 0.40 ± 0.05 meV compared to an activation energy of $\sim$0.1 meV for conductivity activation to a mobility edge at carrier densities $>1.55 \times 10^{11}$ cm^{-2}. Insulating behaviour can occur from a system that behaves as though it is in a minimum metallic state, albeit at high temperature, or from a conductivity greater than a minimum metallic state behaviour showing that local disorder conditions with local differences in the density of states are important for the onset of localization. In the presence of a high magnetic field, thermally activated conductivity is present down to Landau level filling factor $<1/2$ but without a magnetic-field-dependent carrier density or a variable range hopping (VRH) transport behaviour developing even with conductivity $\ll e^2\,h^{-1}$. In the localized transport regime in *p*-type doped $Ge_{0.92}Sn_{0.08}$ QWs the VRH mechanism is suppressed at temperatures >100 mK and this makes this two-dimensional system ideal for future many body localization studies in disordered hole gases that can be thermally isolated from a temperature reservoir.

Keywords: localization, Ge–Sn alloys, electrical transport, high magnetic fields

(Some figures may appear in colour only in the online journal)

1. Introduction

In the development of understanding electron transport in disordered systems an early proposal from Mott [1] was that there was a mobility edge which separated localized and extended states for spatial dimensions >2. When the Fermi energy (E_F), was at the mobility edge (E_C) the conductivity had a definite value termed the minimum metallic conductivity (σ_{min}) and when the Fermi energy was below the mobility edge the conductivity dropped discontinuously to zero at low temperature. The sequence of events was that as the disorder at E_F increased so the scattering increased and the system passed from a Drude conductivity description into the Ioffe–Regel [2] regime where the crystal momentum (k) was no longer a good quantum number as $\Delta k \sim k$ in the strong scattering regime. Further increase of disorder resulted in the onset of the Anderson criterion [3] for localization where E_F was at the mobility edge with conductivity σ_{min}. According to Mott σ_{min} had a value which depended on the Anderson criterion but was near $0.1 \times e^2\,\hbar^{-1} \times a$ in three dimensions (3D) with a the separation of the localized states in real space, e the

* Authors to whom any correspondence should be addressed.

electronic charge and $\hbar$ the reduced Planck's constant. In a two-dimensional (2D) system $\sigma_{\min}$ was constant with value $0.1 \times e^2\ \hbar^{-1}$. Early experiments with considerable localization were in agreement with this prediction, particularly in 2D and a small temperature dependence in conductance was observed above $\sigma_{\min}$. An important aspect of the work when states at E_F were localized was the conduction mechanism (s). When conduction was by thermal excitation to extended states at temperature (T), the conductivity σ is given by equation (1) with the power index $q = 1$,

$$\sigma(T) = \sigma_o e^{-\left(\frac{T_o}{T}\right)^q} \quad (1)$$

where σ_o is the high temperature conductivity intercept and $k_B T_o$ is the thermal activation energy, with k_B Boltzmann's constant and $k_B T_o = E_C - E_F$ in the case of $q = 1$ for thermally activated transport. At lower temperatures conduction was either by variable range hopping (VRH) of Mott [4], $q = 1/3$ or Efros–Shklovskii type [5] where $q = 1/2$. As a result of subsequent theory and experiment it is now known that $\sigma_{\min}$ only exists as a concept and all states in 2D are localized [6] by quantum backscattering but as the localization length becomes macroscopically long so inelastic scattering will break it up and give the appearance of extended state behaviour. Mott's initial treatment assumed that the phase coherence length (L_ϕ) of a wavefunction varied randomly from site to site and therefore quantized backscattering could not occur as the scattering length (l_e) was equal to L_ϕ. However as L_ϕ at very low temperatures was due to electron–electron scattering the factor a in the 3D expression increased, reducing $\sigma_{\min}$ towards zero.

In 2D quantum backscattering reduced the conductivity towards zero but at accessible temperatures produced a logarithmic correction [7]. If the disorder was very weak then it is possible for $l_e > L_\phi$ at accessible temperatures so giving the appearance of an absence of localization and a true metal–insulator–transition. However if $L_\phi > l_e$ but a temperature dependent screening caused the resistivity to decrease with decreasing temperature, the existence of both the quantum back-scattering and the Altshuler–Aronov corrections could be observed in the low field magneto-resistance and the Hall effect. This implied that if temperatures much closer to zero could be obtained then the true localization of all states would be observed.

In this work we investigate the hole transport properties of p-type doped $Ge_{0.92}Sn_{0.08}$ quantum wells (QWs) in an metal–insulator–semiconductor device where characteristics of strong localization are observed including a conductivity close to $\sigma_{\min}$ and thermally activated conductivity. We label the experimental conductivity intercept as σ_m in this paper to avoid confusion with $\sigma_{\min}$ discussed above. The layout of this paper is in the following sections. In section 2 we provide details of device fabrication and subsequent electrical transport measurements in section 3. In section 4 we present experimental data from four different cryostat systems where a set of three devices were measured, each device in at least two of the cryostats. Section 5 is a discussion of the experimental results and implications for the strong localization in this material system and section 6 contains the conclusions of this work.

2. Fabrication of GeSn devices

Details of the material considerations [8] and the device potential have been reviewed [9] for Si-based GeSn structures. A schematic of the device measured in this publication is shown in figure 1(a) with the composition of the wafer structure indicated. The $Ge_{0.92}Sn_{0.08}$ part of the device is a strained QW for holes with Ge barriers, modulation doped with boron acceptors. Three previous [10–12] have described the growth and properties of $Ge_{1-x}Sn_x$ wafers from the same reduced pressure chemical vapour deposition growth reactor. The QW composition, $Ge_{0.92}Sn_{0.08}$ was confirmed *ex-situ* by secondary ion mass spectroscopy (SIMS). The boron modulation doping is in the inverted configuration and low levels of segregation into the QW occur, although SIMS indicates $<3 \times 10^{16}$ cm^{-3} residual boron dopant in the QW albeit close to the SIMS sensitivity limit. Gul *et al* [11] discusses the influence of potential disorder on the transport properties of GeSn QWs in the metallic regime with hole density (p) $\sim 4 \times 10^{11}$ cm^{-2}.

The Ti–Au top gate was insulated by 65 nm of Al_2O_3 dielectric grown at 150 °C with no gate leakage current from V_g (gate voltage) −0.5 to +1.5 V. The device capacitance was typically $\sim$2.5–3.0 $\times$ 10^{11} cm^{-2} $\times$ $V_g{}^{-1}$, with a threshold voltage in the range of 0.7–2.1 V depending on the device cooling conditions and levels of *in-situ* illumination at low temperature, see figure 1(b). Ohmic contacts were formed from sputtered, high purity Pt. Seven gated devices were fabricated in total and the experimental data presented in this paper is from three devices (1) to (3) with several cooling and measuring sets of data (1) up to (4) on the same device. In addition back-gated devices were fabricated and measured but they were more susceptible to random noise levels particularly in the localized transport regime and not discussed further here.

3. Measurement details

The devices were first measured at 1.5 K to determine the carrier density using the Hall effect up to 5 T. There is a persistent increase in carrier density in these devices with brief illumination at 1.5 K. Illumination also reduces the contact resistance to the device, ensuring relatively noise-free electrical measurements. Figure 1(b) shows the hole density with moderate and full illumination as a function of gate voltage. At lower temperatures the carrier density can be determined from the applied gate voltage calibration. Devices (1) and (2) were measured down to 100 mK in an Oxford Instruments *Triton* dilution refrigerator and with an Oxford Instruments *Teslatron* He3 system down to 270 mK. Device (3) was measured up to 30 T in a polyhelix magnet at 100 mK in the LNCMI, Grenoble. Constant AC currents were used, 90 pA–1 nA at 4–33 Hz. The measured voltage was ideally less than 1 μV μm^{-1} of channel length between ohmic contacts. Measuring resistive

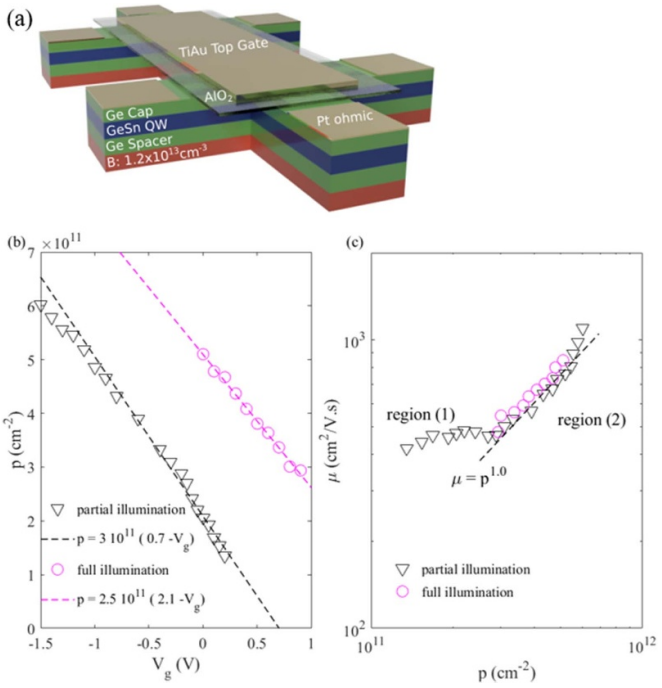

Figure 1. (a) A schematic of the device structure showing the ohmic contact arrangement and the insulated gate region. (b) The carrier density from the Hall effect as a function of top gate voltage for device (1) at 1.5 K. (c) The Hall mobility as a function of carrier density at 1.5 K for device (1) after partial and full illumination conditions. The increase in carrier density with illumination is persistent.

devices close to channel depletion at low temperatures, where the resistivity, $\rho > \sim 3 \times 10^5\ \Omega\ \mathrm{SQR}^{-1}$ can lead to noise problems and the influence of the external circuit on the measured resistance. These effects were minimized by reducing the applied current, measuring at lower frequencies, (4 Hz) and monitoring the out-of-phase components ensuring they are less than the in-phase (resistive) signal components.

4. Experimental results

The device conductivity ($\sigma = 1/\rho$) is determined from the measured resistivity (ρ) in $\Omega\ \mathrm{SQR}^{-1}$ where SQR is the number of squares of material between the voltage probe ohmic contacts of the Hall bar. The mobility (μ) is determined at 1.5 K from the measured conductivity and Hall constant (R_H) with $\mu = \sigma \times R_\mathrm{H}$. The mobility is thermally activated with the same activation energy as the conductivity [11] in these devices. Figure 1(c) shows μ against p at 1.5 K with the partial and full illumination data points in good agreement. There are two regions, (1) $\mu \sim p^0$ and (2) $\mu \sim p^{1.0}$ for $p > 3 \times 10^{11}\ \mathrm{cm}^{-2}$. In region (2) the mobility is limited by background impurity scattering due to the tail of the modulation doped acceptors from the doping layer in the QW. The single particle mobility is not thermally activated and this was previously reported in [11] for GeSn devices and predicted in [13] to result from different scattering mechanisms involved in 2D disordered systems. Region (1) is closer to a mobility that is limited by acoustic phonon scattering and independent of carrier density but temperature dependent. The transport mobility of 400 $\mathrm{cm}^2\ \mathrm{V}^{-1}\ \mathrm{s}^{-1}$ in region (1) is too high to be characteristic of hopping transport. Weak anti-localization signals [14] at low temperature can be seen in these wafers although it does not change the interpretation of what is observed in the strong localization region reported in this paper. The disorder in the devices is coming from the segregation of Sn during the growth process [11]. In addition to this growth-related issue, a short range order prediction [15] may contribute to the localized electronic properties of the underlying GeSn structure.

Figure 2(a) shows the conductivity in device (1) as a function of carrier density at constant temperature from 100 mK to 1 K. The resistivity was measured while sweeping the top gate from 0 to $\sim$+1.0 V. The temperature was then increased from the 100 mK base to $\sim$1 K in incremental steps of 50–100 mK. The conductivity is plotted at constant carrier density as a function of $1/T$ in figure 2(b). The transport mechanism in this device is that of extended state transport by excitation to a mobility edge (induced by a short phase coherence length), where the conductivity is thermally activated and given by equation (1). The dotted lines are fits to equation (1) at constant carrier density, where the parameters, σ_o and T_o can be extracted from fitting. Several features are apparent in the conductivity, such as reproducible fluctuations $\Delta\sigma$ due to the $l_\mathrm{e} < L_\phi$. There is also a region of $p \sim 2 \times 10^{11}\ \mathrm{cm}^{-2}$ at 100 mK where $\mathrm{d}\sigma/\mathrm{d}T$ is <0 rather than $\mathrm{d}\sigma/\mathrm{d}T \sim 0$. This metallic-like behaviour over a small range of carrier density and temperature complicates the simple Anderson localization picture [16] and is not a thermally activated conductivity mechanism.

The lowest measured conductivity is $0.08 \times (e^2\,h^{-1}) \times \mathrm{SQR}$ at $1.55 \times 10^{11}\ \mathrm{cm}^{-2}$ and below this carrier density set by the gate voltage, there is a rapid drop in conductivity that is quantified further in device (2). In figure 3(a) the conductivity in device (2) is shown by sweeping the gate voltage from a carrier density of 1.1–3.4 $\times\ 10^{11}\ \mathrm{cm}^{-2}$ at temperatures down to 270 mK. The same activated behaviour is observed here as in device (1). Figure 3(b) shows the activated conductivity in a clearer fashion on a $1/T$ plot at constant carrier density from 3.4 to 1.1 $\times\ 10^{11}\ \mathrm{cm}^{-2}$ in steps of $\sim$0.2 $\times\ 10^{11}\ \mathrm{cm}^{-2}$. The dotted lines are fits to equation (1) with $q = 1$ where σ_o and T_o are determined. At carrier densities of $<1.55 \times 10^{11}\ \mathrm{cm}^{-2}$ there is a rapid increase in the activation energy to 0.40 $\pm$ 0.05 meV compared to an activation energy of $\sim$0.1 meV in the activated mobility region.

Device (3) was measured in magnetic fields up to 30 T at 100 mK, see figure 4. This figure shows the resistivity (ρ_{xx}) at constant carrier density ($2.9 \times 10^{11}\ \mathrm{cm}^{-2}$) and constant perpendicular magnetic field (B) from 0 T; 12 T (where the filling factor $\upsilon = 1$); to filling factors down to $\upsilon < 1/2$. The filling factor is given by $h \times p/e \times B$ where h is Planck's constant with the other variables already defined. In the heavy hole valence band studied here the valley degeneracy is 1 and the angular momentum $\pm 3/2$ for this band of states. The dotted lines in figure 4 are fits to equation (2)

$$\rho(T) = \rho_\mathrm{o} e^{\left(\frac{T_\mathrm{o}}{T}\right)} \tag{2}$$

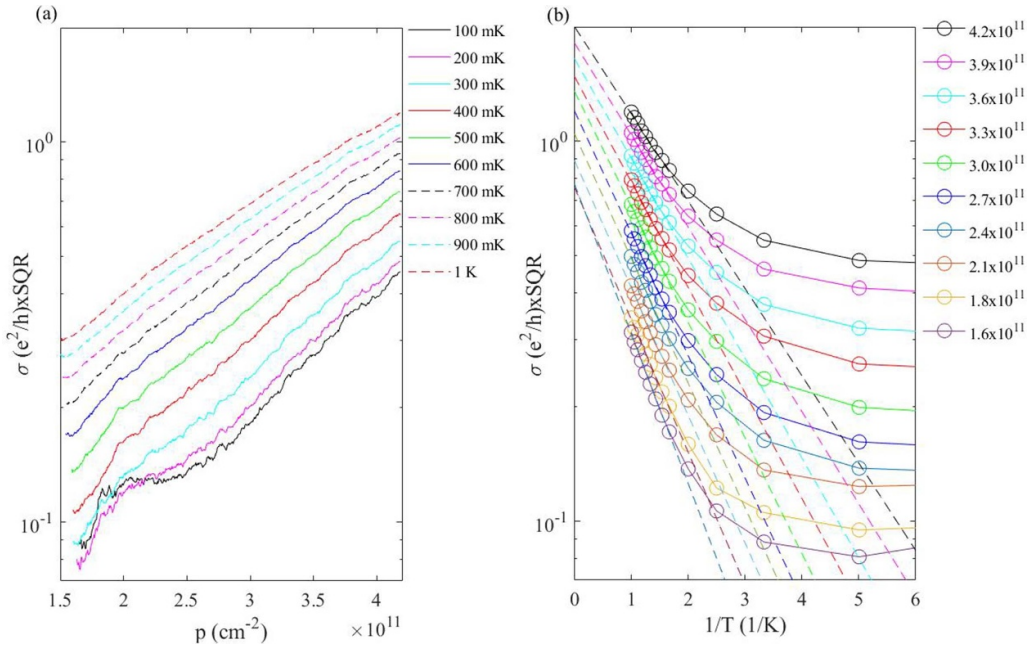

Figure 2. (a) The conductivity as a function of carrier density in device (1) from 100 mK to 1 K. (b) The conductivity as a function of inverse temperature from 4.2 to 1.6 × 10^{11} cm^{-2}.

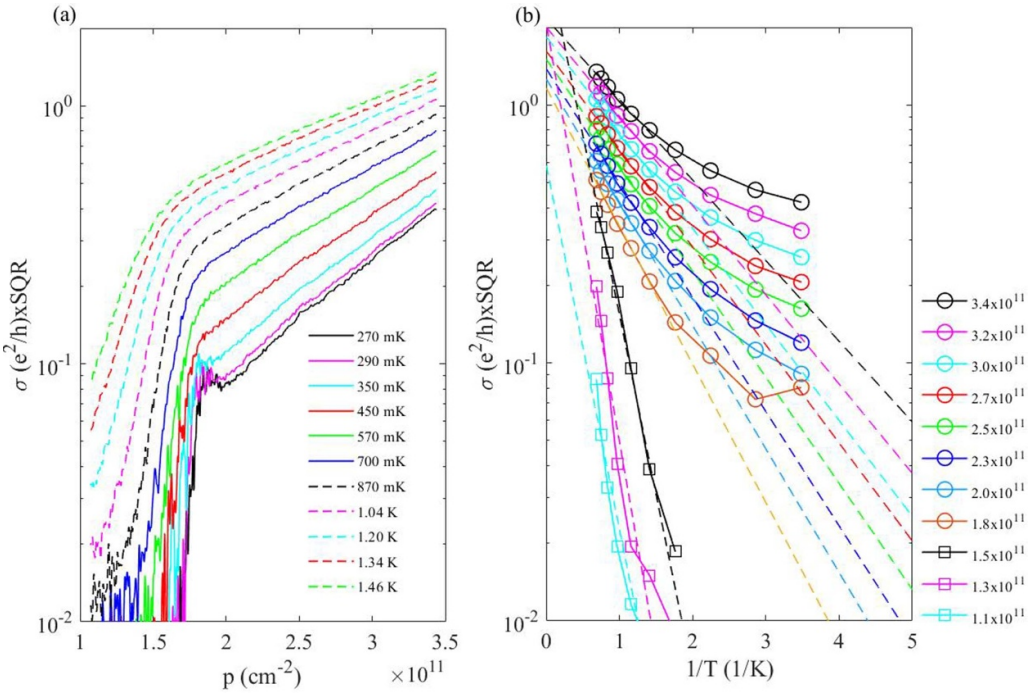

Figure 3. (a) The conductivity as a function of carrier density in device (2) from 270 mK to 1.46 K. (b) The conductivity as a function of inverse temperature at fixed carrier density (3.4–1.1 × 10^{11} cm^{-2}) set by the gate voltage. The fits to the Arrhenius behaviour of equation (2) are shown as dotted lines.

where the intercept ρ_o is $1/\sigma_o$ from equation (1) at zero magnetic field. In this case $\rho_o \approx 1/{\sigma_m}^{-1}$ where $\sigma_m = 0.12 \times (e^2\ \hbar^{-1}) \times$ SQR. T_o at zero magnetic field is 0.89 K which is close to the activation level in device (1) with $p > 1.55 \times 10^{11}$ cm^{-2}. At high magnetic field the intercept ρ_o increases from ${1/\sigma_m}^{-1}$ as expected as the current is confined to the edge of the 2D device. There is no VRH conductivity at any filling factor unlike that seen in [17] or an indication of a magnetic field reduction of the carrier density. A broad $\upsilon = 1$ Shubnikov deHaas effect minimum is seen centred around

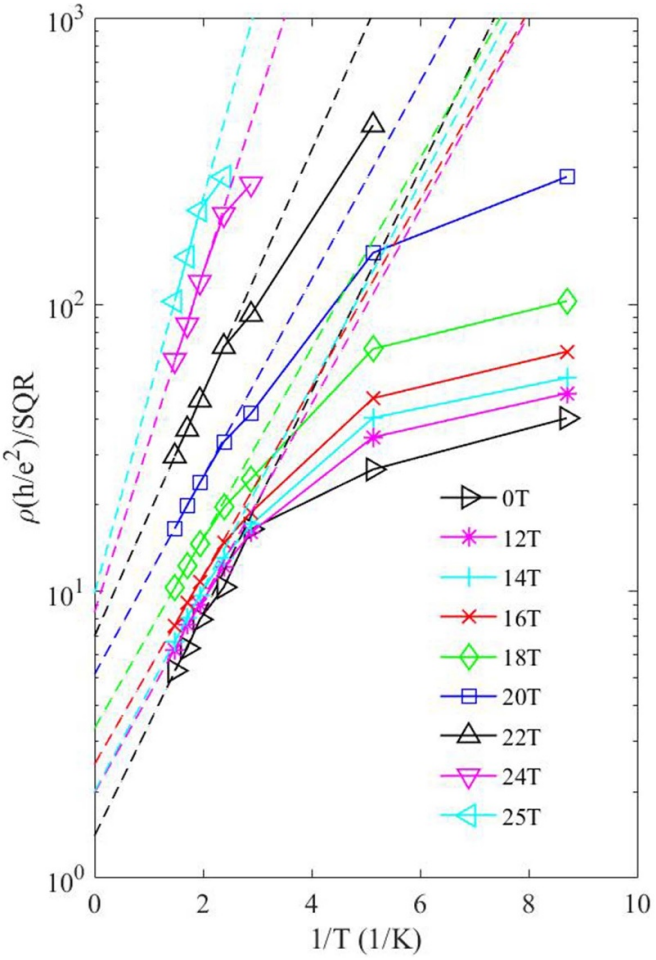

Figure 4. The resistivity as a function of inverse temperature from 0 T to 25 T in device (3) showing conductivity above σ_m at $p = 2.9 \times 10^{11}$ cm^{-2}. The filling factor (ν) = 1 at 12 T.

12 T as the single particle mobility is not thermally activated even with $\rho_{xx} > 1 \times 10^6\ \Omega$ SQR^{-1} ($\sim 40 \times (h\ e^{2-1})$ SQR^{-1}) but the zero field conductivity intercept is at σ_m.

5. Discussion

Figure 5(a) shows the results of fitting equation (1) to the temperature dependent conductivity data for device (1) and (2). The fits are shown as the dotted lines in figures 2(b) and 3(b). There is activated conductivity over four data sets in device (1) and two data sets in device (2). The value of σ_o in units of $(e^2\ h^{-1}) \times$ SQR is plotted as a function of the activation energy $k_B \times (T_o)$ as parameters from equation (1). The *independent variable* in this figure, fit parameter T_o, is driven by the depleting gate voltage that increases the energy difference $(E_C - E_F)$ between the Fermi energy and the mobility edge. The extrapolated σ_o in figure 5(a), (extrapolated from $T_o > 500$ mK) to $T_o = 0$ is $\sim 3.7 \times (e^2\ h^{-1}) \times$ SQR for both devices. This corresponds to the conductivity for the particular doping level at high temperature for the GeSn wafer, irrespective of the particular device. In figure 5(a) the fit parameter σ_o decreases approximately linearly as the fit parameter T_o increases as there is less area of the device to conduct as the Fermi energy is lowered due to percolation of current. There is an abrupt change in behaviour at $\sigma_o = 0.12 \times (e^2\ \hbar^{-1})$ or $0.76 \times (e^2\ h^{-1})$ defined here as σ_m as indicated in figure 5(a), as this constant value of conductivity is approached even with less area of the device available for the percolation of current. This value of fit parameter is then constant even though E_F is reduced closer to the valence band edge as T_o increases. There is no transition to phonon-assisted VRH below σ_m at least down to 100 mK and inelastic scattering never completely dominates the transport behaviour in disordered GeSn. In device (2) there is a similar, approximately linear, decrease of fit parameter σ_o albeit at higher activation energies. The single data point for device (3) is shown at σ_m but with $p = 2.9 \times 10^{11}$ cm^{-2}. The arrows in figure 5(a) indicate the points at which the activation energy increases to 0.40 $\pm$ 0.05 meV (or 4.6 $\pm$ 0.6 K). This is discussed further below with respect to figure 5(b).

The significance of the role played by carrier interaction is characterized by the parameter r_s, which is the ratio of the Coulomb energy to the Fermi energy. In the 2D hole gas, r_s is given by:

$$r_s = \frac{1}{a_o\sqrt{\pi p}} \tag{3}$$

where p is the hole carrier density and a_o is the Bohr radius for a hole in the GeSn valence band. The level of disorder is so strong in the GeSn QWs that r_s is $\sim$1.5 in the strongly localized regime compared to typically $\sim$10. Wigner crystal formation in a 2D hole system [18] occurs at $r_s \sim 40$. In the strongly disordered case the role played by carrier interaction can be included with the concept of Thomas–Fermi screening of the Coulomb potential [19] in this case possibly due to a low level of acceptor impurities in the 2D barrier layers that are screened by mobile holes in the QW. The Coulomb potential $\phi(z)$ from the remote dopant in the barrier layers is screened by the term $e^{-k_{TF}z}$, where k_{TF} is the Thomas–Fermi wave-vector and z is the distance in the growth direction from the remote charged acceptor state to the QW. The Thomas–Fermi wave-vector does not depend on the hole density rather the density of states (DOS) at the Fermi energy D (E_F). In a 2D system the Thomas–Fermi screening wave vector (k_{TF}) is given by:

$$k_{TF} = \frac{e^2}{2\varepsilon} D(E_F) \tag{4}$$

where ε is the dielectric constant. In strictly two-dimensions D (E_F) is constant at $m^*/\pi\hbar^2$ where m^* is the effective mass and correspondingly $k_{TF} = 2/a_o$ with a_o the Bohr radius. In the $Ge_{0.92}Sn_{0.08}$ QWs studied here, a_o is 9.5 nm (based on an $m^* = 0.09 \times m_e$ [11]) and the effective Thomas–Fermi screening wavelength ($2 \times \pi k_{TF}^{-1}$) $\approx$ 30 nm in the metallic regime, i.e. when $\sigma_o > \sigma_m$ from equation (1).

Figure 5(b) shows the activation energy for thermally activated conduction as a function of the carrier density. At a critical hole density (p_c) of 1.55 $\pm$ 0.05 $\times$ 10^{11} cm^{-2} there is a rapid increase in activation energy given by $E_C - E_F$ to 4.6 $\pm$ 0.6 K.

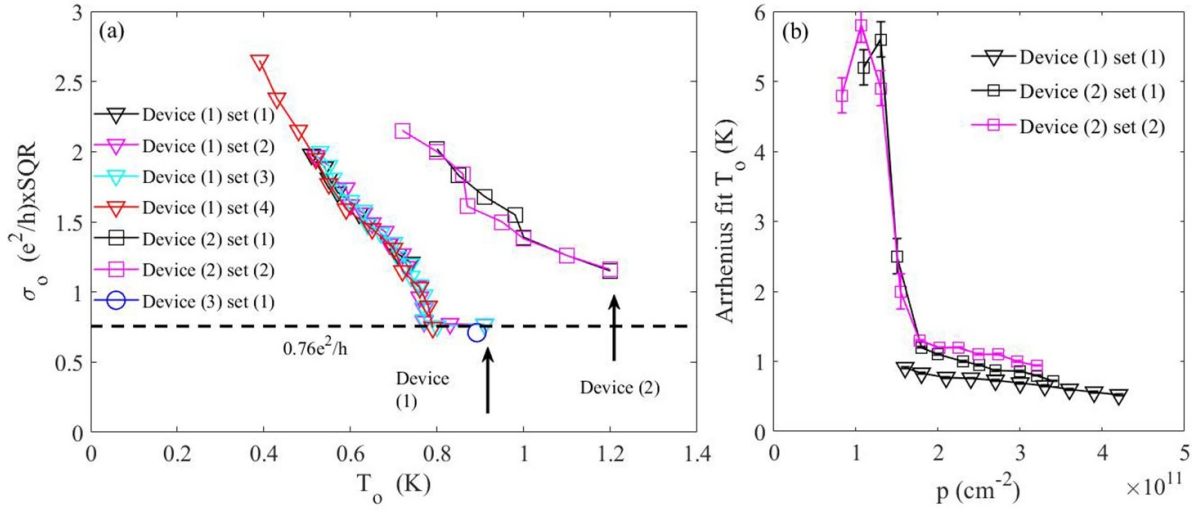

Figure 5. (a) The high temperature conductivity intercept from fitting equation (3) as a function of thermal activation temperature fit for four sets of data from device (1), two sets from device (2) and device (3). σ_m is indicated at $0.76 \times e^2\ h^{-1}$. Device (1) shows strongly localized behaviour (the onset is indicated by the arrow) from σ_m and device (2) shows strongly localized behaviour directly from the metallic regime, $\sigma_o > \sigma_m$. (b) The activation energy of the conductivity as a function of carrier density with the carrier density determined from the Hall effect at 1.5 K.

This behaviour could be due to one of the following (a) to (e) mechanisms:

(a) Transition to a phonon-assisted VRH mechanism at p_c. This would be a conduction mechanism that would fit equation (1) with $q = 1/3$ in the case of Mott VRH or $q = 1/2$ in the case of Efros–Shklovskii VRH. However, the experimental conductance intercept fit $\sigma_o > 5 \times (e^2\ h^{-1}) \times$ SQR for $p < p_c$ and this value is too high for this type of process, where it would be expected to be 1–2 $\times$ $(e^2\ h^{-1}) \times$ SQR for a phonon assisted mechanism [20].

(b) A gap in the DOS at the Fermi energy corresponding to the carrier density p_c. The average DOS at the Fermi energy, $D\ (E_F)$ can be estimated from dp/dw where $w = E_C - E_F$ determined from equation (1). $D\ (E_F)$ is 1.2×10^{14} cm^{-2} eV^{-1} at p_c calculated from dp/dw. This is close to the effective mass value for the DOS of 0.8×10^{14} cm^{-2} eV^{-1} although significantly less than the experimental value of the DOS for $p > p_c$ and $p < p_c$ and hence the description of a gap at p_c. This possible gap in the DOS is not an indication of an Efros–Shklovskii Coulomb gap as the conductance does not fit the VRH mechanism with $q = 1/2$ in equation (1).

(c) A second QW in the Sn-rich segregated region towards the surface of the device. This would account for the apparently higher DOS value compared to the effective mass value at p_c. This is unlikely as it would also interfere with the electrical properties in the metallic regime where a well-defined quantum Hall effect is observed without any parallel conduction mechanism(s) evident [11].

(d) Thermally activated carrier density below p_c. This could be due to a reduction in the Thomas–Fermi screening of the boron modulation doping, residual boron acceptors in the QW or other background impurities, given by equation (4) in the region of reduced DOS at the Fermi energy. This could not be confirmed by Hall effect measurements in this region of carrier density and temperatures below 1.5 K due to the experimental difficulties in obtaining reliable ρ_{xy} values when $\rho_{xx} \sim 10$–$100 \times (h\ e^{-2})$ SQR^{-1}.

(e) A disorder reduced $D\ (E_F)$ in the band tail. This is important, although the concept of a screening parameter given by equation (4) is likely to break down in the strongly localized regime. This has been considered in electron spin resonance measurements in the high mobility SiGe system [21], where a Pauli paramagnetism behaviour results in the experimentally measured magnetic susceptibility being a measure of $D\ (E_F)$ and hence an estimation of k_{TF}. The disorder in the $Ge_{0.92}Sn_{0.08}$ QWs that is caused by Sn-segregation during growth has an approximate Gaussian profile. This distribution of disorder has a strong influence on $D\ (E_F)$ and the Thomas–Fermi screening efficiency as observed in the experimental results reported here. The main difference between the devices (1) and (2) studied here is that in device (1) the strong localization behaviour is directly from a system that behaves as though it is in a minimum metallic state, albeit at high temperature. Device (2) shows strongly localized behaviour directly from a thermally activated conductivity above the metallic conductivity σ_{min} showing that local disorder conditions and local differences in $D\ (E_F)$ are important.

6. Conclusions

Two-dimensional $Ge_{0.92}Sn_{0.08}$ QWs that are modulation doped p-type and fabricated into an metal-oxide-semiconductor (MOS) device show clear localization characteristics. Figure 6 shows an overall summary of the measured conductivity

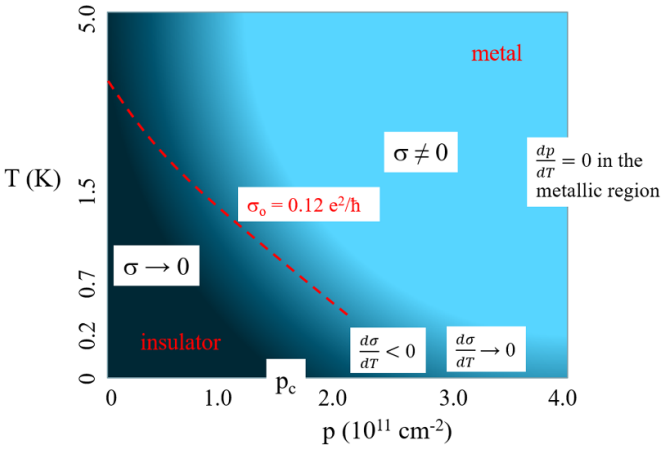

Figure 6. A schematic summary based on the measured conductivity in *p*-type GeSn as a function of carrier density and temperature. Several regions are significant and discussed in the main text: $d\sigma/dT < 0$; $d\sigma/dT \sim 0$; $\sigma_o = \sigma_m$; $\sigma \to 0$. The critical hole concentration p_c is indicated.

behaviour in *p*-type modulation doped $Ge_{0.92}Sn_{0.08}$ QWs as a function of carrier density and temperature. Light blue area is high σ, dark blue is low σ. Several regions have been discussed in previous sections of this publication, with the top right showing metallic behaviour and bottom left insulating behaviour. Above $p = 1.55 \pm 0.05 \times 10^{11}$ cm^{-2} the conductivity is thermally activated and the carrier density is independent of temperature, $dp/dT = 0$, with p set by the gate voltage in the MOS device. At $p < p_c$ then $\sigma \to 0$ at low temperature. There is a region where $d\sigma/dT \sim 0$ above p_c. This is in the metallic region where the Fermi energy is in the band tail and the conduction at this point is with a constant mobility, for example as shown in figure 1(c). The mobility is too high to correspond to a hopping mechanism. With $p \sim 2 \times 10^{11}$ cm^{-2} at low temperature $d\sigma/dT < 0$. This is characteristic of metallic behaviour and has been observed in *p*-type SiGe [16] albeit in the low disorder, high mobility case, although this is unlikely to be operating in the GeSn devices due to the higher levels of disorder in comparison. The red dotted line in figure 6 shows the high temperature intercept conductivity (close to σ_{min}) and below this level $\sigma \to 0$ on reducing the temperature. The disorder energy scale $\hbar/\tau_e$ (where τ_e is the elastic scattering time) is ~32 meV at carrier density 1.55×10^{11} cm^{-2} and this disorder dominates any Coulomb interaction effects with r_s from equation (2) as low as 1.5 in the strongly localized phase below p_c. The lowest measured conductivity is $0.08 \times (e^2\ h^{-1}) \times$ SQR but from the temperature dependence, this is not a VRH conduction mechanism that might be expected [22] even though $\sigma \ll e^2\ h^{-1}$. Applying magnetic fields up to 30 T does not create a magnetic field induced reduction of the carrier density at the minimum conductivity level or a transition to a VRH transport regime. The single particle mobility is not thermally activated unlike the transport mobility and a Shubnikov deHaas effect is clearly observed down to $\upsilon < 1$ with $\rho_{xx} > 10^6\ \Omega$ SQR^{-1}. A conductivity that is thermally activated without entering a Mott VRH regime is ideal for studying many body localization [23] assuming that electron–phonon decoupling can be engineered appropriately.

Data availability statement

The data that support the findings of this study are openly available at the following URL/DOI: https://zenodo.org.

Acknowledgments

This work is supported by an EPSRC (UK) programme Grant Number EP/R029075/1. We also acknowledge the support of the LNCMI-CNRS, member of the European Magnetic Field Laboratory (EMFL) and by the EPSRC (UK) via its membership to the EMFL (Grant No. EP/N01085X/1).

Conflict of interest

The authors have no conflicts of interest to disclose.

ORCID iDs

Y Gul https://orcid.org/0000-0003-2851-1374
S N Holmes https://orcid.org/0000-0002-3221-5124
Chang-Woo Cho https://orcid.org/0000-0002-5190-7070
M Myronov https://orcid.org/0000-0001-7757-2187
M Pepper https://orcid.org/0000-0003-3052-5425

References

[1] Mott N F 1967 *Adv. Phys.* **16** 49
[2] Ioffe A F and Regel A R 1960 *Prog. Semicond.* **4** 237
[3] Anderson P W 1958 *Phys. Rev.* **109** 1492
[4] Mott N F and Davies E A 1971 *Electronic Processes in Non-Crystalline Materials* (Oxford: Oxford University Press)
[5] Efros A L and Shklovskii B I 1975 *J. Phys.* C **8** L49
[6] Abrahams E P, Anderson P W, Licciardello D C and Ramakrishnan T V 1979 *Phys. Rev. Lett.* **42** 673
[7] Uren M J, Davies R A and Pepper M 1980 *J. Phys.* C **13** L985
[8] Kasper E, Werner J, Oehme M, Escoubas S, Burle N and Schulze J 2012 *Thin Solid Films* **520** 3195
[9] Jessica D, Subhajit B, Emmanuele G, Broderick C A, Garcia-Gil A, Duffy R, O'Reilly E P and Holmes J D 2020 *Chem. Mater.* **32** 4383
[10] David W, Jahandar P, Colston G, Allred P, Schulze J and Myronov M 2017 Impact of Sn segregation on $Ge_{1-x}Sn_x$ epi-layers growth by RP-CVD *MIPRO* (*Opatija Croatia, 22–26 May*) (https://doi.org/10.23919/MIPRO.2017.7973388)
[11] Gul Y, Myronov M, Holmes S N and Pepper M 2020 *Phys. Rev. Appl.* **14** 054064
[12] Jahandar P, Weisshaupt D, Colston G, Allred P, Schulze J and Myronov M 2018 *Semicond. Sci. Technol.* **33** 034003
[13] Gold A 1988 *Phys. Rev.* B **38** 10798

[14] David W, Funk H S, Kern M, Dettling M M, Schwarz D, Oehme M, Sürgers C, van Slageren J, Fischer I A and Schulze J 2021 *J. Phys.: Condens. Matter* **33** 085703
[15] Cao B, Chen S, Jin X, Liu J and Li T 2020 *ACS Appl. Mater. Interfaces* **12** 57245
[16] Simmons M Y, Hamilton A R, Pepper M, Linfield E H, Rose P D and Ritchie D A 2000 *Phys. Rev. Lett.* **84** 2489
[17] Briggs A, Guldner Y, Vieren J P, Voos M, Hirtz J P and Razeghi M 1983 *Phys. Rev.* B **27** 6549
[18] Noh H, Lilly M P, Tsui D C, Simmons J A, Hwang E H, Das Sarma S, Pfeiffer L N and West K W 2003 *Phys. Rev.* B **68** 165308
[19] Mott N F 1968 *Rev. Mod. Phys.* **40** 677
[20] Mason W, Kravchenko S V, Bowker G E and Furneaux J E 1995 *Phys. Rev.* B **52** 7857
[21] Wilamowski Z, Sandersfeld N, Jantsch W, Többen D and Schäffler F 2001 *Phys. Rev. Lett.* **87** 026401
[22] Pepper M, Pollitt S, Adkins C J and Oakley R E 1974 *Phys. Lett.* A **47** 71
[23] George M and Lerner Igor V 2021 *Sci. Rep.* **11** 24293